Metallomics

PAPER

Cite this: *Metallomics*, 2016, **8**, 963

Knockdown of copper-transporting ATPase 1 (Atp7a) impairs iron flux in fully-differentiated rat (IEC-6) and human (Caco-2) intestinal epithelial cells†

Jung-Heun Ha,[a] Caglar Doguer[a] and James F. Collins*[ab]

Received 3rd June 2016,
Accepted 22nd August 2016

DOI: 10.1039/c6mt00126b

www.rsc.org/metallomics

Intestinal iron absorption is highly regulated since no mechanism for iron excretion exists. We previously demonstrated that expression of an intestinal copper transporter (Atp7a) increases in parallel with genes encoding iron transporters in the rat duodenal epithelium during iron deprivation (*Am. J. Physiol.: Gastrointest. Liver Physiol.*, 2005, **288**, G964–G971). This led us to postulate that Atp7a may influence intestinal iron flux. Therefore, to test the hypothesis that Atp7a is required for optimal iron transport, we silenced Atp7a in rat IEC-6 and human Caco-2 cells. Iron transport was subsequently quantified in fully-differentiated cells plated on collagen-coated, transwell inserts. Interestingly, ^{59}Fe uptake and efflux were impaired in both cell lines by Atp7a silencing. Concurrent changes in the expression of key iron transport-related genes were also noted in IEC-6 cells. Expression of Dmt1 (the iron importer), Dcytb (an apical membrane ferrireductase) and Fpn1 (the iron exporter) was decreased in Atp7a knockdown (KD) cells. Paradoxically, cell-surface ferrireductase activity increased (>5-fold) in Atp7a KD cells despite decreased Dcytb mRNA expression. Moreover, increased expression (>10-fold) of hephaestin (an iron oxidase involved in iron efflux) was associated with increased ferroxidase activity in KD cells. Increases in ferrireductase and ferroxidase activity may be compensatory responses to increase iron flux. In summary, in these reductionist models of the mammalian intestinal epithelium, Atp7a KD altered expression of iron transporters and impaired iron flux. Since Atp7a is a copper transporter, it is a logical supposition that perturbations in intracellular copper homeostasis underlie the noted biologic changes in these cell lines.

Significance to metallomics

Maintenance of iron homeostasis is essential, since iron deficiency and iron overload have dire pathophysiological outcomes. Humans cannot excrete excess iron, so regulation of iron absorption from the diet ultimately determines overall body iron status. Understanding the intricacies of intestinal iron transport may thus allow the development of pharmacological approaches to alter systemic iron levels in common disease states (*e.g.* iron-deficiency anemia and hereditary hemochromatosis). Furthermore, tissue copper levels vary inversely with iron status (*e.g.* in intestinal mucosa, blood and liver), suggesting that copper may influence iron metabolism. Elucidating mechanisms by which Atp7a (and/or copper) influences intestinal iron flux will therefore provide novel insight into this important physiologic process.

Introduction

Iron is an essential trace mineral that is required for numerous biological functions in mammals. Absorption of iron occurs in the proximal small intestine. Regulation of this process is critical since no active iron excretory systems exist in humans. The intestine thus plays a major physiologic role in overall body iron homeostasis. Numerous recent investigations have contributed to our knowledge of the mechanisms by which dietary iron is absorbed. Although adult humans derive some iron from animal foods as heme iron, most dietary iron is in the form of inorganic (or nonheme) iron. Nonheme iron is derived from animal and plant foods, and this is also the form typically found in supplements and used for fortification of refined grain products. Details of heme iron absorption are still unclear,[1] but the process of nonheme iron absorption has been recently clarified.[2–4] Dietary nonheme iron is in the ferric state,

[a] *Food Science and Human Nutrition Department, University of Florida, Gainesville, Florida, USA*
[b] *Food Science & Human Nutrition Department, University of Florida, Gainesville, FL 32611, USA. E-mail: jfcollins@ufl.edu*

† Electronic supplementary information (ESI) available: See DOI: 10.1039/c6mt00126b

yet ferrous iron enters duodenal enterocytes. Iron reduction occurs via the action of a cell-surface ferrireductase, possibly Dcytb, but other proteins with a similar function may also exist. Ferrous iron is then transported into enterocytes by divalent metal-ion transporter1 (Dmt1). Iron not used for cellular metabolism or stored in ferritin can be transported out of enterocytes by the iron exporter ferroportin 1 (Fpn1). Ferrous iron exported by Fpn1 then requires oxidation for interaction with transferrin in the interstitial fluids. This is likely mediated, at least in part, by the ferroxidase (FOX) hephaestin (Heph), which is present on (or near) the basolateral membrane.

Our previous studies noted that an intestinal copper transporter (copper-transporting ATPase 1 [Atp7a]) was strongly induced in the duodenal epithelium of iron-deprived rats.[5,6] Atp7a functions to pump copper into the *trans*-Golgi network to support cuproenzyme synthesis and it also mediates copper efflux from enterocytes when copper is in excess. Interestingly, Atp7a induction paralleled increases in the expression of genes encoding iron transporters (*e.g.* Dmt1, Fpn1); in fact, the mechanism of induction was shown to be the same, involving a hypoxia-inducible transcription factor, Hif2α.[7–11] Given these facts, it was logical to postulate that copper influences intestinal iron transport. This would, in fact, not be surprising, given the well-established iron-copper interactions in mammals that have been noted previously.[12–14] Exactly how, and if, dietary copper affects intestinal iron absorption has, however, not been definitively established. The current investigation was thus undertaken to test the hypothesis that the Atp7a copper transporter is required for optimal intestinal iron flux. The experimental approach was to utilize reductionist models of the mammalian small intestine, namely cultured intestinal epithelial cells (IECs) derived from rat and human, in which Atp7a expression was silenced using the siRNA technique. After confirmation of significant knockdown of Atp7a mRNA and protein expression, vectorial iron flux was quantified in fully-differentiated cells grown on transwell cell culture inserts. Complementary molecular and functional studies were also performed, allowing us to draw mechanistic conclusions regarding the biologic role of Atp7a (and/or copper) in cellular iron homeostasis.

Methods

Cell culture and development of Atp7a knockdown cell lines

Rat intestinal epithelial (IEC-6) cells (American Type Culture Collection [ATCC]; Manassas, VA; #CRL-1592) were cultured in DMEM (Corning; New York, NY) with 10% FBS (Sigma; St. Louis, MO), 10 U mL^{-1} insulin and 100 U mL^{-1} penicillin/streptomycin (Corning) at 37 °C in a 5% CO_2/95% O_2 atmosphere. Both non-specific (control) and Atp7a-specific shRNA-expressing plasmids (Invitrogen; Carlsbad, CA), which were described previously,[15] were transfected into IEC-6 cells using PolyJet DNA *In Vitro* Transfection Reagent (SignaGen Laboratories; Gaithersburg, MD). Four unique, Atp7a-specific shRNA-expressing plasmids were mixed in equal amounts for transfection. Subsequently, cell cultures were maintained in the presence of 250 μg mL^{-1} zeocin (Thermo Fisher Scientific; Waltham, MA) to select for cells that had been transfected with one or more plasmids. This approach, as opposed to transient transfection with siRNAs, was necessary since all experiments were performed with fully-differentiated (*i.e.* post-confluent) cells. Thereafter, transfected cells were plated at very low density and several unique clonal populations were selected and propagated. Two of these clonal subpopulations, with the most significant Atp7a KD (called KD1 and KD2), were then chosen for further experimentation. This approach ensured that the results of subsequent analyses were not confounded by the genomic insertion site of the plasmid(s), which was presumably different in each of the clonal cell populations.

We also utilized a complementary approach to silence Atp7a in IEC-6 cells, lentiviral plasmid-mediated transfection. Negative-control and Atp7a-targeting lentiviral plasmids (Cat. #TL711714; OriGene; Rockville, MD) were transfected into IEC-6 cells using the transfection kit provided by the manufacturer. Similar to the shRNA-expressing plasmid approach described above, four different Atp7a-targeting lentiviral plasmids were mixed in equal amounts and transfected into cells. Subsequent cell cultures were maintained under antibiotic pressure using 100 μg mL^{-1} puromycin (Research Products International Corp.; Mt Prospect, IL) with selection of 2 distinct clonal cell populations (using the same procedure as described above). Furthermore, to broaden the scope of our investigation, we also generated Atp7a KD Caco-2 cell lines. Caco-2 cells were obtained from ATCC (#HTB-37) and were cultured in MEM with 15% FBS (Sigma) plus 100 U mL^{-1} penicillin/streptomycin (Corning) at 37 °C in a 5% CO_2/95% O_2 atmosphere. Negative-control (cat. #sc-108060) and Atp7a-targeting (sc-105107-SH) lentiviral vector shRNA plasmids (Santa Cruz Biotechnology, Inc.; Dallas, TX) were transfected into Caco-2 cells using PolyJet and then maintained in the presence of the selective agent, puromycin (100 μg mL^{-1}). Two different Atp7a-targeting shRNA plasmids were mixed in equal proportions for transfection and 2 clonal cell populations were selected and propagated (as described above).

All cells were grown in tissue culture-treated polystyrene dishes, or in transwell cell culture inserts (Corning) for mineral analyses and transport assays. For all experiments, differentiated cells were used: IEC-6, 7–8 days post-confluence; Caco-2, 20–21 days. To create iron-deficient conditions, cells were incubated in the presence of 200 μmol L^{-1} deferroxamine (DFO; an iron chelator) (Sigma) for 24 h prior to experimentation. The DFO was removed and the cells were thoroughly washed with PBS prior to performing subsequent analyses. For mRNA decay experiments, 1 μg mL^{-1} Actinomycin D (ActD; Sigma) or vehicle (PBS) was added to the cell culture medium for 0–24 h, and then mRNA and heteronuclear RNA (hnRNA) levels were assessed by qRT-PCR.

Atomic absorption spectroscopy (AAS)

IEC-6 cells were cultured in 6-well plates and cells lysates were prepared in 500 μl of 0.2 N NaOH containing 0.2% SDS and

were digested with 500 μl of HNO_3 at 95 °C for 3 h and then analyzed by flame AAS (AAnalyst 100; Perkin Elmer; Waltham, MA), using a standard protocol. Detection limits of this instrument for iron and copper are 0.1 μg L^{-1}. Digested cell lysates were appropriately diluted so that readings were in the linear phase of detection based on standards with known iron and copper concentrations. Iron and copper concentrations were acquired from the same digested samples. Mineral concentration data were normalized by protein concentration of the individual lysates.

^{59}Fe uptake and efflux studies

1.0×10^6 IEC-6 or Caco-2 cells were seeded onto collagen-coated, polytetrafluoroethylene membrane cell culture inserts (6.5 mm diameter; 0.4 μm pore size) (Corning) in 12-well plates and allowed to fully differentiate. To ensure that the monolayers were intact with fully-formed tight junctions, transepithelial electrical resistance (TEER) and phenol red flux were routinely assessed, as we described previously.[15,16] TEER values were routinely 36–40 Ω cm^{-2} for IEC-6 cells and >250 Ω cm^{-2} for Caco-2 cells. ^{59}Fe uptake and efflux were quantified utilizing a previously reported, standard protocol.[17,18] After transport studies, cells were washed in a buffer containing 150 mmol L^{-1} $NaCl_2$, 10 mmol L^{-1} HEPES (pH 7.0), and 1 mmol L^{-1} EDTA to remove all surface-bound ^{59}Fe. Radioactivity in cell monolayers and in the medium in the basal chamber was determined using a WIZARD^2 Automatic Gamma Counter (Perkin Elmer), and ^{59}Fe uptake and efflux data were normalized by protein concentration of cell lysates.

qRT-PCR

This entire procedure was performed according to routine procedures published previously.[19] Briefly, total RNA was isolated from IEC-6 and Caco-2 cells using RNAzol® RT reagent (Molecular Research Center; Cincinnati, OH). Reverse transcription (iScript cDNA synthesis kit; Bio-Rad; Hercules, CA) was performed using 1 μg of mRNA per individual sample. Gene-specific, oligonucleotide primers (Table S1, ESI†) were designed to span large introns to avoid amplification from genomic DNA,[19] and were used at 1 μmol L^{-1}. Heteronuclear RNA (hnRNA) primers were designed to span exon/intron boundaries. Prior to analysis of hnRNA levels, genomic DNA was removed by DNase I (Thermo-Fisher Scientific) digestion. Gene expression was assessed using SYBR Green, real-time, quantitative PCR (CFX96; Bio-Rad). mRNA expression levels of experimental genes were normalized to the expression of cyclophilin (which did not vary significantly between samples). Relative mRNA decay rates were calculated by taking the difference between the absolute initial Ct values and the Ct values at various time points after Act D treatment. Data were subsequently plotted and a best line fit was applied. The mRNA half-life was then calculated as the time point where the initial mRNA levels had decreased by 50%.

Western blot analysis

Protein lysates from IEC-6 or Caco-2 cells were prepared using ice-cold, radioimmune precipitation assay (RIPA) buffer with protease inhibitors (Thermo-Fisher Scientific). Proteins were separated by 7.5% SDS-PAGE and transferred to polyvinylidene difluoride membranes (Merck Millipore; Billerica, MA) using a standard blotting apparatus (Bio-Rad). Subsequently, blots were incubated with primary and secondary antibodies, developed with enhanced chemiluminescence reagent and protein bands were detected using a FluorChem E imaging system (Cell Biosciences; San Jose, CA). The following primary and secondary antibodies were used: Atp7a (1 : 1000 dilution) (produced in-house[6]); Dmt1 (1 : 1000) (sc-30120; Santa Cruz); Fpn1 (1 : 100) (sc-49668; Santa Cruz); Heph (1 : 100) (sc-49970; Santa Cruz); HIF2α (1 : 1000) (NB100-122; Novus Biologicals; Littleton, CO); α-tubulin (1 : 5000) (ab6046; Abcam, UK). After an overnight incubation with a respective primary antibody at 4 °C, blots were incubated with anti-IgG rabbit secondary antibody (1 : 3000; A120-101P; Bethyl Laboratories; Montgomery, TX) or donkey anti-goat IgG (1 : 2000; sc-2020; Santa Cruz) diluted in 5% milk containing tris-buffered saline and tween 20 for 1 h at room temperature. The optical density of immunoreactive bands on images was determined using ImageJ (http://imagej.nih.gov/ij/download.html) and experimental protein band intensity was normalized to the intensity of the α-tubulin immunoreactive band.

Ferrireductase and ferroxidase activity assays

Ferrireductase activity. IEC-6 cells were fully differentiated in 24-well cell culture plates and then incubated in Krebs-Ringer buffer for 30 min in a cell culture incubator. Cells were then incubated with 2 mmol L^{-1} nitrotetrazolium blue (NTB) (Sigma) in Krebs-Ringer buffer at 37 °C for 90 min. NTB is a membrane impermeant electron acceptor that allows quantification of redox reactions. Cells were then washed 3 times with Krebs-Ringer buffer and images were subsequently captured using an EVOS XL Core Cell Imaging system (Thermo-Fisher Scientific). After acquiring images, isopropanol was added and the blue color intensity of the isopropanol wash was determined at 560 nm using a Synergy H1 plate reader (BioTek; Winooski, VT).

Ferroxidase activity. Transferrin-coupled FOX activity assays were performed as described previously,[20,21] using cytosolic and membrane proteins[20] purified from control and Atp7a KD IEC-6 cells. Initial reaction velocities were measured from 5 to 120 s by reading absorbance at 460 nm using a spectrophotometer (Implen GmbH, Germany) at room temperature. Blanks (excluding protein) were used to control for autoxidation of iron, and all experimental data were normalized to the baseline data from the blanks.

Statistical analysis

Results are presented as means ± SDs. All analyses were performed using GraphPad Prism (version 6.0 for Windows). The trends in data were analyzed using a One-way ANOVA test followed by Tukey's multiple comparisons test.

Results

Atp7a knockdown perturbs iron and copper homeostasis in IEC-6 cells

To understand the role of Atp7a in iron homeostasis, Atp7a expression was silenced in IEC-6 cells, using two independent methods, and also in Caco-2 cells. Atp7a KD by stable transfection of shRNA-expressing plasmids was confirmed at the mRNA (>70% reduction) and protein (>60%) levels in IEC-6 cells (Fig. 1A and B). Atp7a KD was also confirmed in IEC-6 cells transfected with Atp7a-targeting lentiviral plasmid vectors and in Caco-2 cells (Fig. S1, ESI†). To assess the impact of Atp7a KD on intracellular iron and copper homeostasis, control and Atp7a KD IEC-6 cells were cultured and fully differentiated in the transwell system, and then, intracellular iron and copper concentrations were assessed by AAS. Atp7a KD cells contained lower concentrations of iron and copper under basal conditions (Fig. 1C). These data indicate that Atp7a is involved not only in cellular copper homeostasis, but that Atp7a activity also influences iron metabolism.

Atp7a knockdown inhibits vectorial iron transport in IEC-6 and Caco-2 cells

To determine whether Atp7a is required for optimal iron flux, control and Atp7a KD cells were cultured and fully differentiated on collagen-coated, transwell inserts for 8 (IEC-6) or 21 (Caco-2) days and iron transport assays were performed. ^{59}Fe accumulation (uptake) and efflux were determined by assessing accumulation of radioactivity in cells and in the basal chamber after a 90 min transport period. Atp7a KD in IEC-6 cells resulted in significantly decreased ^{59}Fe uptake and efflux in basal (~70%), and iron-deficient (~85%) conditions created by DFO treatment (Fig. 2A and B). Furthermore, additional iron transport studies in IEC-6 and Caco-2 cells with Atp7a silenced using lentiviral shRNA-expressing plasmids confirmed these observations: ^{59}Fe uptake into and efflux from cells was impaired without fully functional Atp7a (Fig. 2C–F). Importantly, transport data represented specific, active transport processes since TEER values were in the specified range for all assays and moreover, very low amounts of ^{59}Fe appeared in the basal chambers (<0.2% of total radioactive counts added to the apical chamber). These data convincingly demonstrate that Atp7a is required for optimal iron transport in these 2 *in vitro* models of the mammalian small intestinal epithelium. Impairment of iron uptake is consistent with the fact that Atp7a KD cells had lower intracellular iron content (see Fig. 1C). Moreover, inhibition of iron transport occurred in the setting of decreased intracellular copper concentrations, suggesting that copper may be positively associated with iron transport.

Atp7a KD alters expression of genes and proteins related to iron homeostasis

Atp7a KD in IEC-6 cells perturbs iron and copper homeostasis and also impairs vectorial iron flux. Additional experiments were thus designed to elucidate the molecular underpinnings of these observations. We first assessed expression of genes encoding the brush-border membrane (BBM) and basolateral membrane (BLM) iron transport machinery using qRT-PCR. Expression of Dcytb and Dmt1 was attenuated by Atp7a KD under basal conditions (Fig. 3A and B). Dcytb expression was

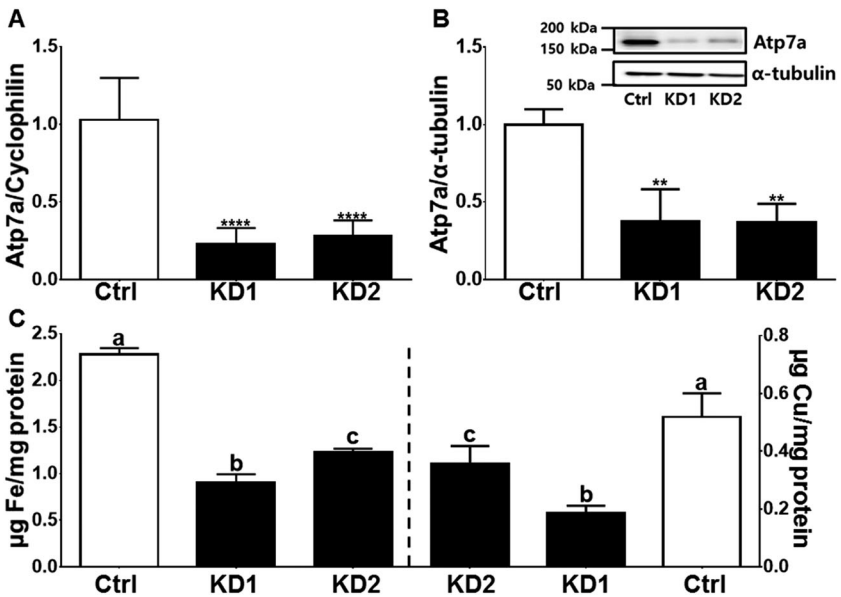

Fig. 1 Atp7a knockdown impairs iron and copper homeostasis in IEC-6 cells. IEC-6 cells were transfected with a negative-control (Ctrl) (scrambled) or Atp7a-targeting, shRNA-expressing plasmids. 2 clonal knockdown (KD) cell populations were selected (KD1, KD2). Atp7a KD was verified at the mRNA (A) and protein (B) levels in fully-differentiated cells. A representative western blot is shown (B, inset). Intracellular iron and copper (C) concentrations were quantified by AAS in fully differentiated Ctrl and Atp7a KD IEC-6 cells. Values are means ± SDs. Data were analyzed by One-way ANOVA followed by Tukey's *post hoc* analysis. $^{**}p < 0.01$ and $^{****}p < 0.0001$, as compared to control values (A and B). Labeled means without a common letter differ ($p < 0.05$) (C). n = 3 independent experiments with 3 technical replicates per experiment.

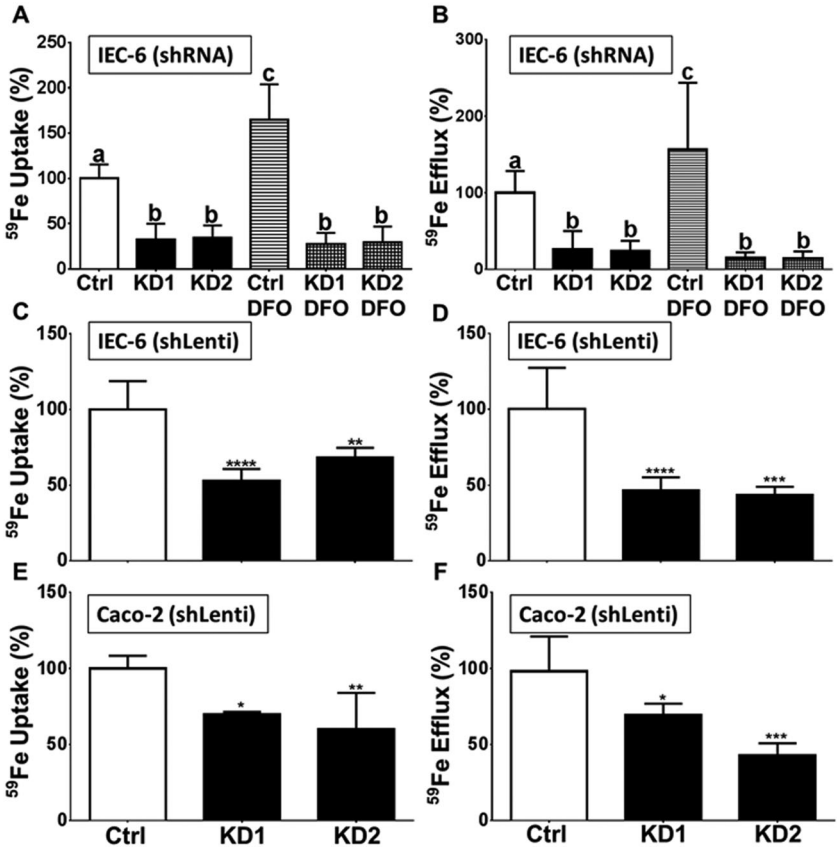

Fig. 2 Atp7a silencing impairs transepithelial iron flux in IEC-6 and Caco-2 cells. Ctrl and Atp7a KD IEC-6 and Caco-2 cells were grown on collagen-coated, transwell cell-culture inserts for 8 (IEC-6) or 21 (Caco-2) days. In some experiments, 200 μmol L^{-1} deferroxamine (DFO) (or vehicle, PBS) was added to the apical and basolateral medium of cultured IEC-6 cells for the last 24 h to create iron-deficient conditions. Subsequently, 0.5 μmol L^{-1} ^{59}Fe-citrate in uptake buffer was added to the apical chamber at 37 °C and uptake was allowed to proceed for 90 min. ^{59}Fe accumulation (uptake) (A, C and E) and efflux (B, D and E) to the basolateral chamber were then determined by gamma counting. ^{59}Fe uptake and efflux were normalized to the protein concentration of individual cell lysates. Values are means ± SDs. Data were analyzed by One-way ANOVA followed by Tukey's *post hoc* analysis. Labeled means without a common letter differ ($p < 0.05$) (A and B). *$p < 0.05$, **$p < 0.01$, ***$p < 0.0005$ and ****$p < 0.0001$, as compared to control values (C–F). n = 3 independent experiments with 3 technical replicates per experiment.

also low under iron-deprived conditions, while Dmt1 expression was similar to control values after DFO treatment. Expression of Fpn1 was also diminished in Atp7a KD cells under basal and iron-deprived conditions (Fig. 3C). Conversely, expression of Heph was dramatically increased in Atp7a KD cells, but expression was unaffected by DFO treatment (Fig. 3D). Expression of a BBM copper transporter (copper transporter 1 [Ctr1]) was also diminished significantly by Atp7a KD, but expression was unaffected by DFO treatment (Fig. 3E). Moreover, despite noted alterations in intracellular copper concentrations, expression of metallothionein 1a mRNA (encoding a copper-binding protein) was unaffected by Atp7a KD (Fig. S3, ESI†). Also, transferrin receptor 1 (Tfr1) expression increased significantly in all DFO-treated cells, confirming the iron-deprived condition since the Tfr1 transcript is stabilized by low intracellular iron (Fig. 3F).

To validate observations relating to mRNA levels in Atp7a KD cells, we next assessed protein expression by immunoblot analysis. Dmt1 and Fpn1 protein expression levels were decreased significantly in Atp7a KD cells, in agreement with the mRNA expression data (Fig. 4A and B). Also, Heph protein levels were higher in KD cells (Fig. 4C), again exemplifying the relevance of the mRNA expression data. Moreover, since several intestinal genes related to iron transport are induced by a hypoxia-inducible factor (Hif2α) during iron deficiency, we also quantified Hif2α protein levels in control and Atp7a KD cells. Hif2α protein expression was diminished by Atp7a KD, possibly providing a mechanistic explanation for the decrease in Dcytb, Dmt1 and Fpn1 expression, given that all of these genes are known to be regulated by this transcription factor. Reductions in Dmt1, Fpn1 and Hif2α and increases in Heph protein expression were also confirmed in the other IEC-6 Atp7a KD cell lines (which were created using lentiviral technology) (Fig. S2, ESI†). Overall, these data demonstrate that lack of Atp7a leads to decreased expression of BBM and BLM iron and copper transport-related genes and proteins, likely contributing to the decreases in intracellular iron and copper concentrations and impaired transepithelial iron flux noted in these cells. Moreover, it is a logical assumption that increases in Heph expression represent a compensatory response to maximize iron flux.

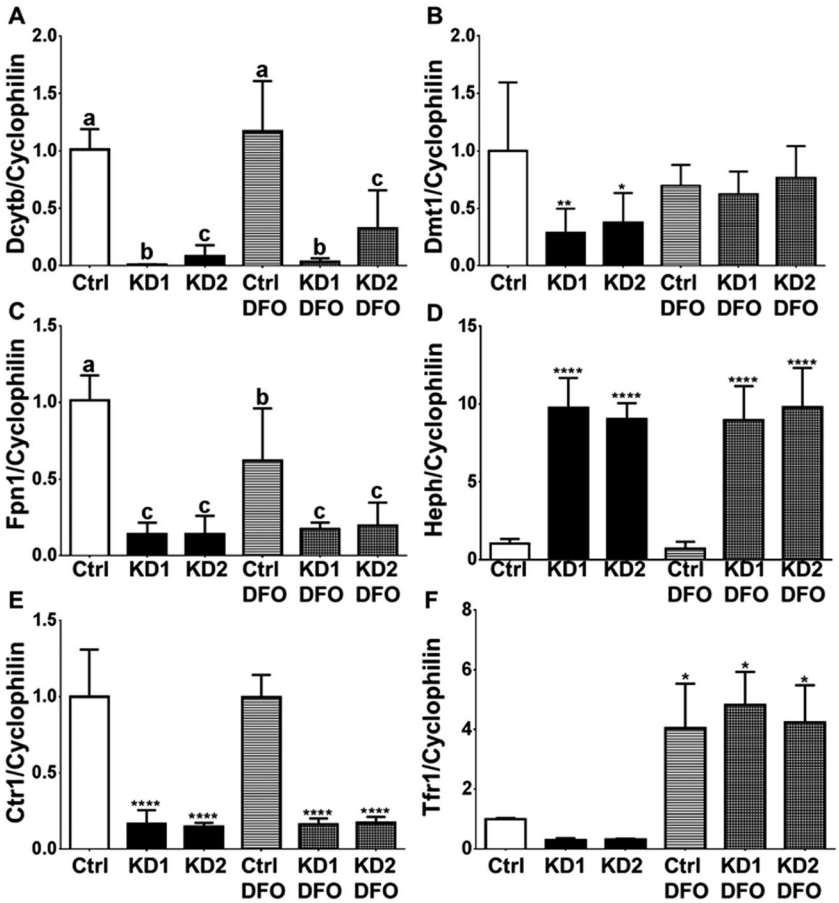

Fig. 3 Atp7a KD alters expression of iron homeostasis-related genes. mRNA was purified from fully-differentiated Ctrl or Atp7a KD IEC-6 cells and SYBR-Green qRT-PCR was performed to quantify expression of iron and copper transport-related genes. 200 μmol L^{-1} DFO was added to some wells for the last 24 hours to create an iron-deficient condition. Induction of transferrin receptor 1 (Tfr1) confirmed iron deficiency (F). Values are means ± SDs. Data were analyzed by One-way ANOVA followed by Tukey's *post hoc* analysis. Labeled means without a common letter differ ($p < 0.05$) (A and C). *$p < 0.05$, **$p < 0.01$ and ****$p < 0.0001$, as compared to other groups (B, D–F). $n = 3$ independent experiments with 3 technical replicates per experiment.

Atp7a KD alters transcription rates and mRNA stability

To elucidate the mechanism by which Atp7a KD influences expression of genes related to iron transport, we next performed experiments to assess gene transcription and mRNA decay rates (indicative of mRNA stability). Unspliced, nuclear RNA (or heteronuclear RNA [hnRNA]) represents the initial output of transcription of a gene; quantification of hnRNA levels thus reflects transcription initiation rates. Experiments were designed to directly compare hnRNA and mRNA expression levels of genes showing the most significant alterations in Atp7a KD cells. Confirming data presented in Fig. 3, Dcytb and Fpn1 mRNA levels were decreased significantly in KD cells (Fig. 5A and C). Interestingly, Dcytb and Fpn1 hnRNA levels were intermediate between control and Atp7a KD mRNA levels, suggesting that changes in mRNA levels relate to transcriptional and post-transcriptional regulatory events. One possibility was that the mRNA transcripts are less stable in KD cells. Therefore, transcription was inhibited for various times with ActD, and transcript levels were quantified by qRT-PCR. The half-lives ($t_{1/2}$; the time when 50% of the transcripts have been degraded) of Dcytb and Fpn1 transcripts were not different when comparing control to KD cells (Fig. 5B and D). Changes in message stability are thus unlikely to contribute to the greater magnitude of decrease in mRNA levels as compared to hnRNA levels. Furthermore, Heph mRNA levels were confirmed to increase significantly in Atp7a KD cells, yet Heph hnRNA levels were identical in control and KD cells (Fig. 5E). These data suggested that post-transcriptional mechanisms contribute to the noted increases in Heph mRNA in the KD cells. Again, however, the decay rate of Heph mRNA transcripts was not different between control and KD cells (Fig. 5F). Thus, Heph transcription rates and transcript stability were not altered in the KD cells, so other post-transcriptional mechanisms would have to be invoked to explain the dramatic increase in transcript levels (*e.g.* alterations in pre-mRNA splicing or nuclear export). In sum, these data demonstrate that lack of fully functional Atp7a causes complex molecular changes in cells that lead to alterations in the expression of the *Dcytb*, *Fpn1* and *Heph* genes.

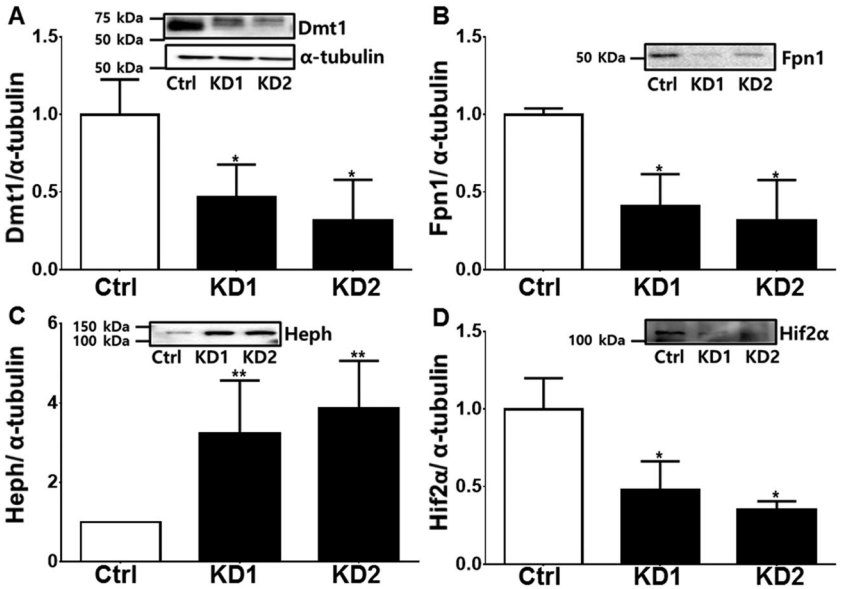

Fig. 4 Atp7a silencing alters expression of iron transport-related proteins. Ctrl or Atp7a KD IEC-6 cells were grown for 8 days post-confluence and then total cell lysates were prepared for western blot analysis. α-Tubulin was used as an internal standard. Each blot was cut into strips and probed with different antibodies, since all proteins have distinct molecular weights (so α-tubulin is shown only once in panel A). The Fpn1 antibody detected several bands, which all decreased similarly in KD cells in a pilot experiment, but only the one of the correct m.w. (~54 kDa) is shown and quantified. Quantitative data from 3 independent experiments is shown in each panel, with a representative western blot shown as an inset. Values are means ± SDs. Data were analyzed by One-way ANOVA followed by Tukey's *post hoc* analysis. *$p < 0.05$, and **$p < 0.01$, as compared to other groups (A–D). n = 3 independent experiments.

Atp7a KD enhances cell-surface ferrireductase and membrane and cytosolic ferroxidase activity in IEC-6 cells

Dietary nonheme iron is in the ferric state, yet ferrous iron is imported into duodenal enterocytes by Dmt1. Iron must thus be reduced, which is likely mediated by one or more cell-surface ferrireductases. In Atp7a KD cells, Dcytb mRNA expression was diminished significantly, so it was a logical next step to assess reductase activity in this model. Unexpectedly, reductase activity was significantly enhanced in both Atp7a KD IEC-6 cell populations (Fig. 6). Since NTB is a non-specific electron acceptor, we cannot definitively conclude, however, that the noted redox activity was the result of a ferrireductase. It would be logical to include though that at least some portion of this activity was due to the action of a ferrireductase. Moreover, since Heph mRNA and protein expression was induced in Atp7a KD IEC-6 cells, we measured membrane and cytosolic FOX activity. We previously demonstrated that Heph and non-Heph FOXs exist in the membranes and cytosolic fractions of cultured IECs and also in rat duodenal enterocytes.[20,21] Consistent with Heph mRNA and protein expression data, FOX activity was enhanced in membrane and cytosolic fractions of Atp7a KD cell lines (Fig. 7). Increases in reductase and FOX activity may thus represent compensatory mechanisms to maximize iron flux when expression of iron transporters is attenuated.

Discussion

Previous studies provided rationale for considering whether the Atp7a copper transporter, and by inference copper, is involved in the regulation of intestinal iron transport.[5,6] For example, we demonstrated that the Atp7a gene is induced by Hif2α during iron deprivation/hypoxia in IEC-6 cells.[7,8] Importantly, this same regulatory mechanism induces expression of several genes encoding proteins involved in intestinal iron transport. Furthermore, it is well established that body copper is redistributed during iron deprivation, with hepatic and serum copper levels being notably higher. Increased hepatic copper may result in accelerated biosynthesis and secretion of ceruloplasmin by hepatocytes and higher serum FOX activity,[22] which presumably potentiates iron release from stores. What is not known, however, is the molecular mechanism(s) responsible for altering copper distribution. One possibility is that increased intestinal Atp7a activity positively influences copper homeostasis, thus promoting intestinal iron absorption. The current investigation was thus designed to directly test the role of Atp7a in vectorial iron transport.

Diminution of Atp7a expression and (presumably) activity impaired iron flux in fully-differentiated IEC-6 and Caco-2 cells. Lack of Atp7a also prevented the increase in iron transport caused by iron deprivation in IEC-6 cells. Reduced iron transport was associated with decreases in Dcytb, Dmt1 and Fpn1 mRNA and protein expression. Moreover, Hif2α protein levels were lower in Atp7a KD cells. Whether Hif2α plays a direct role in transcription of these genes under basal conditions is not known, but it is well established that Hif2α is required for induction of intestinal iron transport during iron deficiency. Lack of Hif2α could thus, conceivably, be responsible for the decrease in expression of Dcytb, Dmt1 and Fpn1. It was further experimentally established that at least part of the decrease in

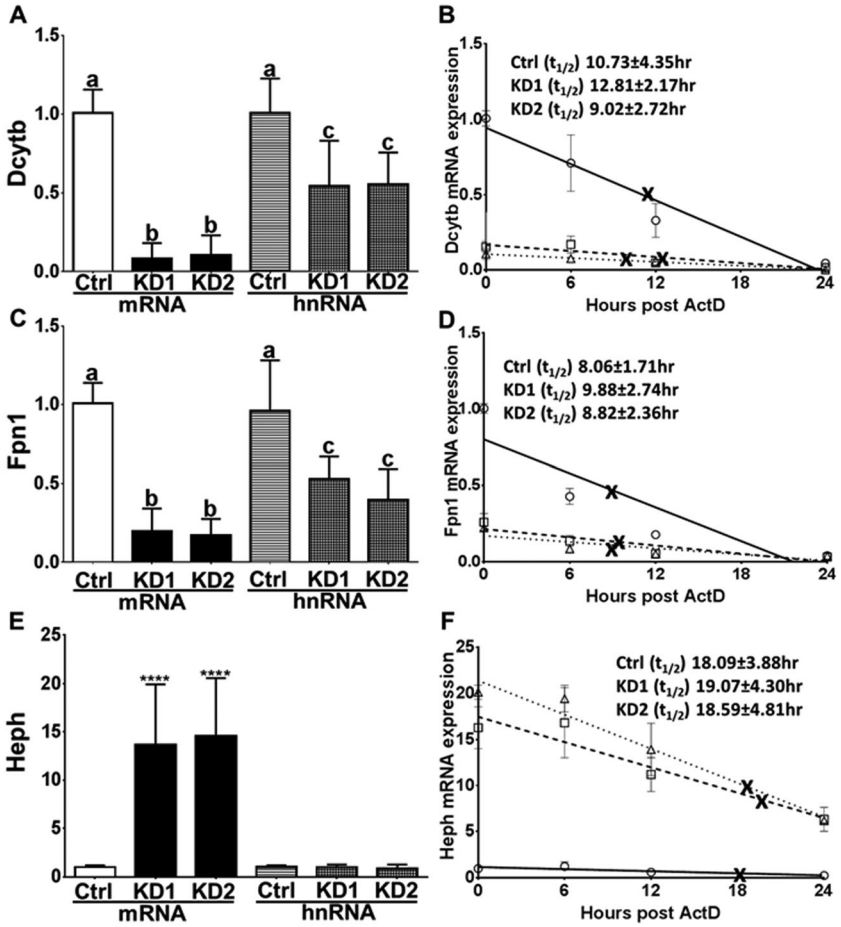

Fig. 5 Atp7a KD causes transcriptional and posttranscriptional effects on the expression of iron transport-related genes. Total RNA, including mRNA and heteronuclear RNA (hnRNA), was harvested from fully-differentiated Ctrl or Atp7a KD IEC-6 cells and then gene expression levels were quantified by qRT-PCR (panels A, C and E). To quantify mRNA half-lives, cells were treated with actinomycin D (ActD) for 0, 6, 12 or 24 hours prior to cell harvest and then qRT-PCR was performed with gene-specific primers (panels B, D and F). Line fits were performed for data points for each gene and cell population. The mRNA half-life for each transcript is indicated with an "x", which has been placed at the approximate position where the starting mRNA levels were reduced by 50% (actual times [$t_{1/2}$] are indicated as insets in each panel). Values are means ± SDs. Data were analyzed by One-way ANOVA followed by Tukey's *post hoc* analysis. Labeled means without a common letter differ ($p < 0.05$) (A and C). ****$p < 0.0001$, as compared to other groups (E). $n = 6$ (mRNA and hnRNA quantification) or $n = 3$ (mRNA decay) independent experiments with 3 technical replicates per experiment.

Dcytb and Fpn1 mRNA levels related to perturbed gene transcription, further supporting a possible role for Hif2α.

In the setting of decreased Dcytb mRNA and protein expression in Atp7a KD cells, surprisingly, there was an induction of cell-surface reductase activity. This observation supports the notion that additional ferrireductases exist in IECs and is also consistent with the lack of a notable phenotype in the Dcytb KO mouse,[23] including no noted defect in intestinal iron absorption. The increase in reductase activity could represent a compensatory mechanism to maximize iron intake *via* Dmt1. Furthermore, Heph mRNA and protein levels were increased significantly in Atp7a KD cells. This was associated with enhanced FOX activity in cytosolic and membrane fractions of the cells. Like the noted increase in ferrireductase activity, this may be a compensatory response to increase iron efflux, since iron oxidation is thought to be functionally coupled to export by Fpn1.

The final important point relates to the *in vivo* significance of the current data. Our original observation was that Atp7a was one of the most robustly induced genes in the duodenal epithelium of iron-deficient rats at several different post-natal ages.[5] Atp7a protein expression also increased dramatically under these conditions.[6] In rats, induction of Atp7a correlates nicely with increases in tissue copper levels during iron deprivation, perhaps representing one mechanism by which copper is redistributed. Our hypothesis is that Atp7a function in enterocytes promotes vectorial iron flux, a supposition which is supported by the current investigation. A predictable mechanism by which this could occur relates to the possible potentiation of the biosynthesis of the multi-copper FOX Heph, given that Atp7a function supports the production of cuproenzymes. The current data, do not, however, support this contention as Heph expression and FOX activity was enhanced by Atp7a KD. Furthermore, Atp7a KO rats are not currently available to test the *in vivo* significance of Atp7a in iron metabolism. An intestine-specific Atp7a KO mouse was, however, recently developed.[24] In this model, no changes in iron metabolism were noted, but this was not the specific hypothesis

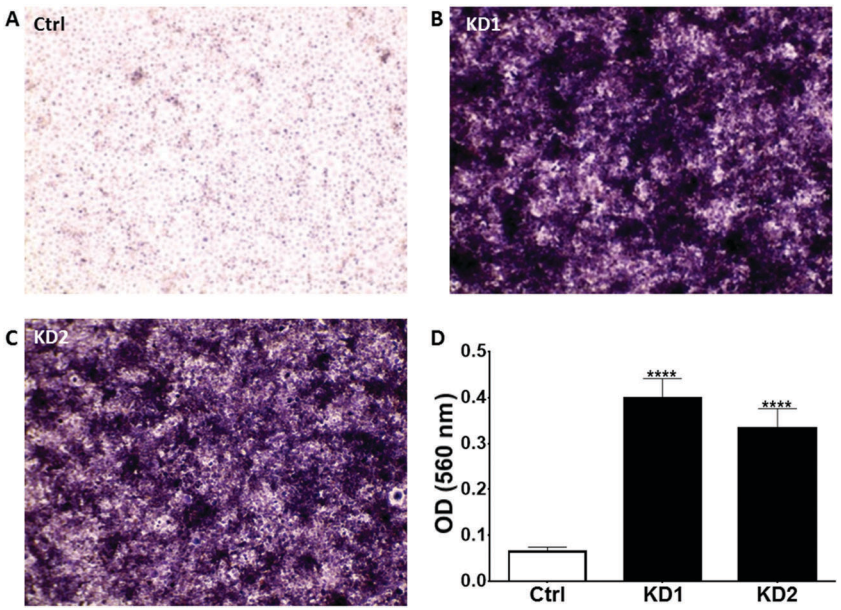

Fig. 6 Atp7a KD enhances cell-surface ferrireductase activity in IEC-6 cells. Fully-differentiated Ctrl or Atp7a KD IEC-6 cells were treated with nitrotetrazolium blue (NTB). Color intensity, indicative of ferrireductase activity, was determined by spectrophotometric measurement of isopropanol eluates. Representative pictures are shown from Ctrl (A) or Atp7a KD (B and C) cells along with color intensity quantification of isopropanol eluates from all experiments (D). Values are means ± SDs (D). Data were analyzed by One-way ANOVA followed by Tukey's *post hoc* analysis. ****$p < 0.0001$, as compared to the control value. $n = 4$ independent experiments.

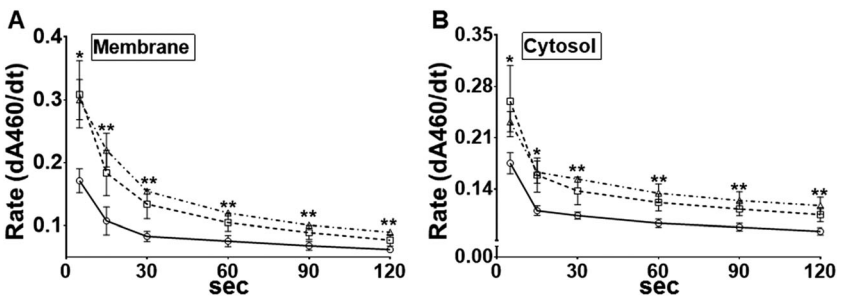

Fig. 7 Atp7a KD increases membrane and cytosolic ferroxidase activity in IEC-6 cells. Membrane and cytosolic proteins were isolated from fully-differentiated Ctrl or Atp7a KD IEC-6 cells, and FOX activity was determined by an *apo*-transferrin-coupled assay from membrane (A) and cytosolic (B) proteins for 5–120 seconds. KD1 and KD2 were statistically identical. Asterisks indicate statistical differences from Ctrl values (*$p < 0.05$; ** $p < 0.01$) (One-way ANOVA followed by Tukey's *post hoc* analysis). $n = 3$ independent experiments.

being tested. Nonetheless, we are not surprised by this observation since copper redistribution in response to changes in iron metabolism has not been reported frequently in mice, as it has in numerous other mammalian species including humans.[13] Mice may thus be outliers in regards to the influence of copper on iron metabolism.[12] Lastly, the current observations in the Caco-2 cell model are consistent with the noted alterations in copper homeostasis during perturbations of iron metabolism in humans. Future *in vivo* experimentation is, however, required to confirm the present *in vitro* findings.

Conclusions

Experimental evidence presented in this paper provides strong evidence of a supportive role for Atp7a and/or copper in intestinal iron transport. This is important since the intestine plays a seminal role in the control of overall body iron homeostasis. The Atp7a copper transporter, which we show is required for expression of iron transporters and for functional iron transport, is emerging as a potential mediator of iron metabolism. The significance of the current investigation is limited by the *in vitro* models used, but is supportive of *in vivo* observations made in rats and humans. A definitive test of the role of Atp7a in intestinal iron homeostasis will thus await the development of an Atp7a mutant rat line.

Acknowledgements

This work was supported by National Institutes of Health grant R01 DK074867 (J. F. C.).

References

1 S. Gulec, G. J. Anderson and J. F. Collins, *Am. J. Physiol.: Gastrointest. Liver Physiol.*, 2014, **307**, G397–G409.
2 D. M. Frazer and G. J. Anderson, *Am. J. Physiol.: Gastrointest. Liver Physiol.*, 2005, **289**, G631–G635.
3 B. K. Fuqua, C. D. Vulpe and G. J. Anderson, *J. Trace Elem. Med. Biol.*, 2012, **26**, 115–119.
4 B. Mackenzie and M. D. Garrick, *Am. J. Physiol.: Gastrointest. Liver Physiol.*, 2005, **289**, G981–G986.
5 J. F. Collins, C. A. Franck, K. V. Kowdley and F. K. Ghishan, *Am. J. Physiol.: Gastrointest. Liver Physiol.*, 2005, **288**, G964–G971.
6 J. J. Ravia, R. M. Stephen, F. K. Ghishan and J. F. Collins, *J. Biol. Chem.*, 2005, **280**, 36221–36227.
7 L. Xie and J. F. Collins, *Am. J. Physiol.: Cell Physiol.*, 2011, **300**, C1298–C1305.
8 L. Xie and J. F. Collins, *J. Biol. Chem.*, 2013, **288**, 23943–23952.
9 M. Mastrogiannaki, P. Matak, B. Keith, M. C. Simon, S. Vaulont and C. Peyssonnaux, *J. Clin. Invest.*, 2009, **119**, 1159–1166.
10 Y. M. Shah, T. Matsubara, S. Ito, S. H. Yim and F. J. Gonzalez, *Cell Metab.*, 2009, **9**, 152–164.
11 M. Taylor, A. Qu, E. R. Anderson, T. Matsubara, A. Martin, F. J. Gonzalez and Y. M. Shah, *Gastroenterology*, 2011, **140**, 2044–2055.
12 S. Gulec and J. F. Collins, *Annu. Rev. Nutr.*, 2014, **34**, 95–116.
13 P. L. Fox, *BioMetals*, 2003, **16**, 9–40.
14 J. F. Collins, J. R. Prohaska and M. D. Knutson, *Nutr. Rev.*, 2010, **68**, 133–147.
15 S. Gulec and J. F. Collins, *J. Nutr.*, 2014, **144**, 12–19.
16 D. A. Gaitán, S. Flores, F. Pizarro, M. Olivares, M. Suazo and M. Arredondo, *Biol. Trace Elem. Res.*, 2012, **145**, 300–303.
17 M. C. Linder, N. R. Zerounian, M. Moriya and R. Malpe, *BioMetals*, 2003, **16**, 145–160.
18 O. Han and M. Wessling-Resnick, *Am. J. Physiol.: Gastrointest. Liver Physiol.*, 2002, **282**, G527–533.
19 J. F. Collins, Z. Hu, P. N. Ranganathan, D. Feng, L. M. Garrick, M. D. Garrick and R. W. Browne, *Am. J. Physiol.: Gastrointest. Liver Physiol.*, 2008, **294**, G948–G962.
20 P. N. Ranganathan, Y. Lu, B. K. Fuqua and J. F. Collins, *BioMetals*, 2012, **25**, 687–695.
21 P. N. Ranganathan, Y. Lu, B. K. Fuqua and J. F. Collins, *Proc. Natl. Acad. Sci. U. S. A.*, 2012, **109**, 3564–3569.
22 P. N. Ranganathan, Y. Lu, L. Jiang, C. Kim and J. F. Collins, *Blood*, 2011, **118**, 3146–3153.
23 H. Gunshin, C. N. Starr, C. Direnzo, M. D. Fleming, J. Jin, E. L. Greer, V. M. Sellers, S. M. Galica and N. C. Andrews, *Blood*, 2005, **106**, 2879–2883.
24 Y. Wang, S. Zhu, V. Hodgkinson, J. R. Prohaska, G. A. Weisman, J. D. Gitlin and M. J. Petris, *Am. J. Physiol.: Gastrointest. Liver Physiol.*, 2012, **303**, G1236–G1244.